Available online at www.sciencedirect.com
SCIENCE DIRECT®
PERGAMON
Electrochimica Acta 48 (2003) 711–720
ELECTROCHIMICA Acta
www.elsevier.com/locate/electacta

In situ FTIR monitoring of Ag and Au electrodeposition on glassy carbon and silicon

K. Márquez [a,*,1], R. Ortiz [b,1], J.W. Schultze [a,1], O.P. Márquez [b,1], J. Márquez [b,1], G. Staikov [a,1]

[a] *Institut für Physikalische Chemie und Elektrochemie, Heinrich-Heine-Universität Düsseldorf, Universitätsstraße 1, Geb. 26.32, 40225 Düsseldorf, Germany*
[b] *Departamento de Química Facultad de Ciencias, Laboratorio de Electroquímica, Universidad de los Andes, Mérida 5101, Venezuela*

Received 14 October 2002; received in revised form 13 November 2002

Abstract

Formation of Ag, Au and Ag–Au alloys on Si and Glassy Carbon (GC) electrodes from alkaline cyanide electrolytes was investigated using a combination of electrochemical and spectroscopic techniques. Metal deposition and dissolution processes could be studied in situ by monitoring the ν(CN) bands of the metal complexes and the free cyanide ion in the region between 2000 and 2200 cm^{-1} using FTIR reflectance spectroscopy. Under the experimental conditions, two different silver complexes, namely $[Ag(CN)_2]^-$ and $[Ag(CN)_3]^{2-}$ (whilst only one gold complex, namely $[Au(CN)_2]^-$), were identified. In the case of the Ag–Au alloys, both species co-deposit even in the activation region, where Ag reduction is expected to be the main reaction. Experimental results indicate that in a mixed electrolyte containing equal amounts of Ag and Au, Ag deposition is thermodynamically favoured ($E^0_{eq,\,Ag} > E^0_{eq,\,Au}$), while Au deposition is kinetically favoured. The Ag–Au alloy deposition follows a progressive nucleation mechanism even at relatively high negative potentials. The morphology and adhesion of all deposits, as well as the alloy composition, were found to be strongly dependent on the deposition conditions. A better adhesion of the films with a higher Au content was observed, due to the formation of a more stable Au–Si bond.

Keywords: Electrodeposition; FTIR; Silver; Gold; Silicon; Glassy carbon; Alloys

1. Introduction

Metallisation on silicon plays a key role in the production of integrated devices. In the last years, metal and alloy electrodeposition has attracted more attention as a versatile technique for tailoring ohmic contacts and Schottky barriers. Due to the stringent demands in modern technologies, many conventional materials (i.e. aluminium alloys) cannot keep pace as building blocks for the ever narrower and more densely packed interconnecting lines. The application of copper for electronic devices may also be limited due to the undesired diffusion of this metal into the Si substrate and to its poor binding to the surface of the semiconductor [1,2]. Therefore, other materials are being intensively researched for this purpose, and in this context metals such as Ag and Au, as well as their alloys, exhibit quite interesting characteristics. These metals do not diffuse into Si, thus avoiding the need for barrier seed layers; and they have very high electrical conductivities, forming covalent bonds with Si that improve their adhesion to the semiconductor surface [3–5]. Unfortunately, most of the non-cyanide based electrolytes for Ag and Au deposition are relatively unstable and the properties of the metal films obtained in cyanide-free solutions are generally poor. Because of this, non-cyanide Ag- and Au-plating processes are still not well accepted [6]. However, due to environmental reasons, only relatively low cyanide concentrations are normally used in industrial processes.

* Corresponding Author. Tel.: +49-211-8114152; fax: +49-211-8112803.
E-mail address: marquez@uni-duesseldorf.de (K. Márquez).
[1] ISE Member (K. Márquez: Student member).

0013-4686/02/$ - see front matter
PII: S0013-4686(02)00740-5

In general, the structure and properties of the resulting metal and alloy films are strongly dependent on the mechanism of nucleation and growth. Therefore, a detailed understanding of the processes occurring during electrodeposition is crucial for obtaining high quality deposits [7].

In the last few years many spectroelectrochemical methods have shown their importance for studying the electrode/electrolyte interfacial region. Undoubtedly, a very successful technique has been potential modulated external reflectance IR spectroscopy [8], in which both spectral and transient information about the concentrations of absorbing species in the diffusion layer at the electrode can be obtained. In the last years, reflectance Fourier Transform IR spectroscopy has been successfully applied for studying various electrochemical systems [9–12].

In this paper, a study of the electrodeposition of Ag, Au and Ag–Au alloys on H-terminated n-type silicon (111) from cyanide solutions is presented and compared with results obtained on glassy carbon (GC). The deposition process on both substrates was investigated using a combination of electrochemical and spectroscopic methods. For obtaining continuous and smooth deposits, a double pulse polarisation routine, previously described [13], was used. Some physical and electronic properties of the deposits, which have been studied using combined surface analytical and electrochemical techniques are also briefly discussed.

2. Experimental

Electrochemical measurements were carried out in a conventional three-electrodes cell at room temperature in the systems:

a) n-Si(111)/x mM AgCN + 0.2 M KCN + 0.5 M KOH (pH 14);
b) n-Si(111)/x mM AuCN + 0.2 M KCN + 0.5 M KOH (pH 14);
c) n-Si(111)/x mM AgCN + x mM AuCN + 0.2 M KCN + 0.5 M KOH (pH 14);
d) GC/x mM AgCN + 0.2 M KCN + 0.5 M KOH (pH 14);
e) GC/x mM AuCN + 0.2 M KCN + 0.5 M KOH (pH 14); and
f) GC/x mM AgCN + x mM AuCN + 0.2 M KCN + 0.5 M KOH (pH 14).

Electrolyte solutions were prepared from analytical grade chemicals and Millipore® water and kept under inert atmosphere. For the in situ spectroelectrochemical studies, a typical external reflectance cell with a flat CaF_2 window was used. A 2000 FTIR Spectrometer (Perkin–Elmer) with a software-controlled source carousel and a liquid nitrogen cooled Mercury Cadmium Telluride (MCT) detector was coupled to the electrochemical system for the FTIR measurements [14]. Wavelength reference was provided by a 632.99 nm helium neon (He/Ne) laser. For data manipulation, a difference protocol was adopted, with only those absorptions that changed with time and/or potential being retained in the spectra: the reference spectrum, S_r, was collected at a reference potential, E_r, within an electro-inactive region. Then, depending on the case, the potential was either successively stepped to other values (E_s), being further spectra (S_s) collected at each step, or it was changed in a single potential increment and the spectra S_s were collected as a function of time. The number of averaged scans was chosen to give an adequate signal/noise ratio. All spectra are presented as:

$$\Delta R/R = (S_s - S_r)/S_r \text{ versus } \nu \text{ (cm}^{-1}\text{)} \quad (1)$$

Experiments were performed either on phosphorous-doped n-Si(111) wafers (Silchem, Germany) with a resistivity of 7.5 Ω cm ($N_D \approx 10^{15}$ cm^{-3}) or on GC discs (HTW, Germany). Prior to each experiment the Si wafers were sequentially cleaned ultrasonically for 10 min in trichloroethylene, acetone, ethanol and water. An ohmic contact was formed on the back side of the wafer by applying InGa eutectic after treatment in 48% HF and 40% NH_4F for 2 min. After this treatment a stepped hydrogen-terminated Si surface with atomically flat terraces was obtained. The GC discs were first polished with several grades of alumina (Buehler) down to 0.3 μm, then cleaned in Millipore® water in an ultrasonic bath for 10 min and finally pre-treated electrochemically in the metal-free solutions. All electrode potentials given here are referred to the standard hydrogen electrode (SHE).

3. Results and discussion

Typical cyclic voltammograms in the systems: n-Si/$[Ag(CN)_2]^-$, n-Si/$[Au(CN)_2]^-$ and n-Si/$[Au(CN)_2]^-$ + $[Ag(CN)_2]^-$ are shown in Fig. 1. In all cases cyclic voltammograms show initial deposition peaks and limiting current densities, indicating a mass transport controlled deposition process at high negative potentials. Ag behaves as a more noble metal than Au in this medium, and a difference of about 150 mV is observed between both deposition peaks (Fig. 1a). In the case of the mixed Ag–Au electrolyte (Fig. 1b), electrodeposition starts earlier than deposition of Ag or Au from the corresponding one component electrolytes, indicating a strong interaction between adsorbed Ag and Au species. However, the nucleation and growth kinetics from a solution containing equal amounts of AgCN and AuCN is afterwards slightly inhibited, the deposition peak being shifted in about $\Delta E = 110$ mV to more negative

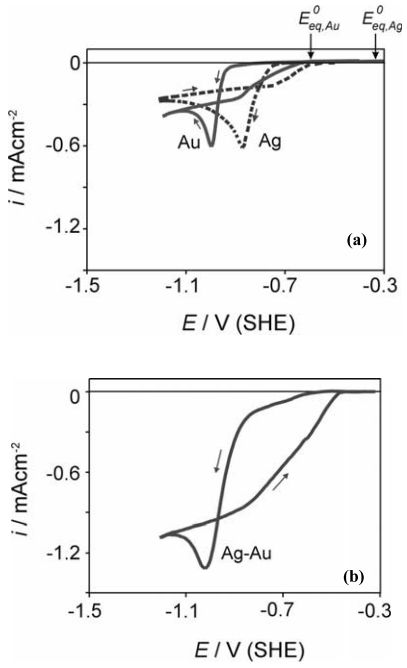

Fig. 1. Cyclic voltammograms for: (a) Ag and Au deposition in the systems: n-Si(111)/$[Ag(CN)_2]^-$ (pH 14, $c_{AgCN} = 5$ mM) and n-Si(111)/$[Au(CN)_2]^-$ (pH 14, $c_{AuCN} = 5$ mM). Scan rate $|dE/dt| = 10$ mV/s. The standard equilibrium potentials ($E^0_{eq,\ Ag}$ and $E^0_{eq,\ Au}$) for the systems Ag/$[Ag(CN)_2]^-$ and Au/$[Au(CN)_2]^-$ are shown. (b) Alloy deposition in the system n-Si(111)/$[Ag(CN)_2]^-$ + $[Au(CN)_2]^-$ (pH 14, $c_{AgCN} = c_{AuCN} = 5$ mM). Scan rate $|dE/dt| = 10$ mV/s.

potentials with respect to the system: n-Si/$[Ag(CN)_2]^-$. Due to the formation of high Schottky barriers in all cases [13], the deposits cannot be dissolved electrochemically under the experimental conditions. For comparison, curves in the systems: GC/$[Ag(CN)_2]^-$, GC/$[Au(CN)_2]^-$ and GC/$[Ag(CN)_2]^-$ + $[Au/(CN)_2]^-$ are presented in Fig. 2a and b. Metal and alloy deposits can be easily dissolved from the GC electrode and equivalent charge densities were estimated for the deposition and dissolution processes in all cases. As it can be seen in Fig. 2a, Ag deposition on GC takes place at a less negative potential than on Si. In the case of Au (Fig. 2a), a small dissolution peak is observed at $E = -0.43$ V in the cyclic voltammogram in addition to the main dissolution peak. As reported by MacArthur [15], this smaller peak could be consistent with a charge transfer reaction, producing an intermediate ($AuCN_{ads}$) which becomes soluble by a rate-determining chemical reaction in which the species $[Au(CN)_2]^-$ is finally formed. In Fig. 2b, a cyclic voltammogram obtained during the alloy deposition, showing both dissolution peaks for Ag and Au, can be seen. Fig. 2c shows cyclic voltammograms taken at two different scanning rates during Ag–Au alloy deposition on GC. As can be seen, at $dE/dt = 10$ mV/s both anodic peaks corresponding to Ag and Au dissolution can be clearly distinguished, while at $dE/dt = 50$ mV/s only the peak for Au dissolution is well defined. These results suggest that the amount of Ag deposited at higher sweep rates is relatively small compared to Au, indicating a higher Au deposition rate. EDX and XPS measurements performed on Ag–Au alloy deposits formed at different scanning rates on n-Si(111) confirm these observations [16].

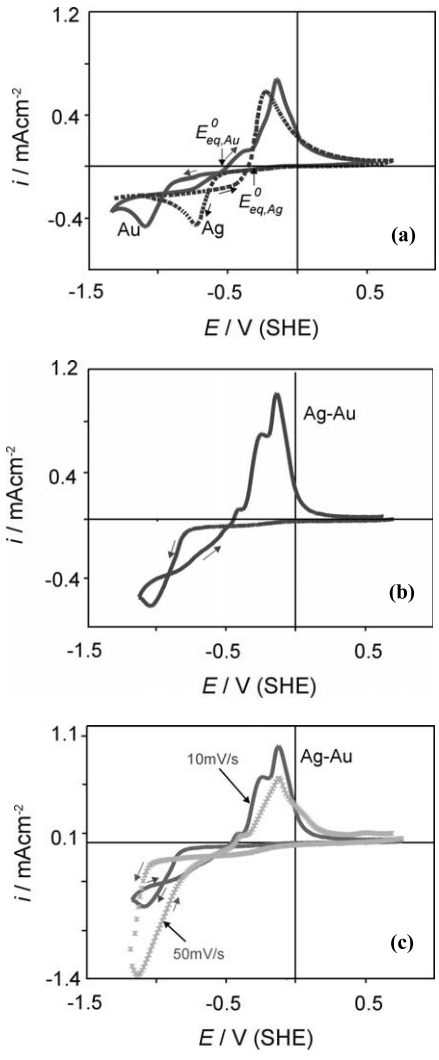

Fig. 2. Cyclic voltammograms for: (a) Ag and Au deposition in the systems: GC/$[Ag(CN)_2]^-$ (pH 14, $c_{AgCN} = 5$ mM) and GC/$[Au(CN)_2]^-$ (pH 14, $c_{AuCN} = 5$ mM). Scan rate $|dE/dt| = 10$ mV/s. The standard equilibrium potentials ($E^0_{eq,\ Ag}$ and $E^0_{eq,\ Au}$) for the systems Ag/$[Ag(CN)_2]^-$ and Au/$[Au(CN)_2]^-$ are shown. (b) Alloy deposition in the system GC/$[Ag(CN)_2]^-$ + $[Au(CN)_2]^-$ (pH 14, $c_{AgCN} = c_{AuCN} = 5$ mM). Scan rate $|dE/dt| = 10$ mV/s; (c) Alloy deposition in the system GC/$[Ag(CN)_2]^-$ + $[Au(CN)_2]^-$ (pH 14, $c_{AgCN} = c_{AuCN} = 5$ mM). Scan rates $|dE/dt| = 10$ and 50 mV/s.

Upon coordination to a metal, the vibration band of the CN^- group, which is normally found at about 2080 cm^{-1}, shifts to higher frequencies. Additionally, the C–N stretching bands in cyano complexes are governed by the electronegativity, the oxidation state and the coordination number of the metal. Because of this, it is possible to distinguish very well between the different

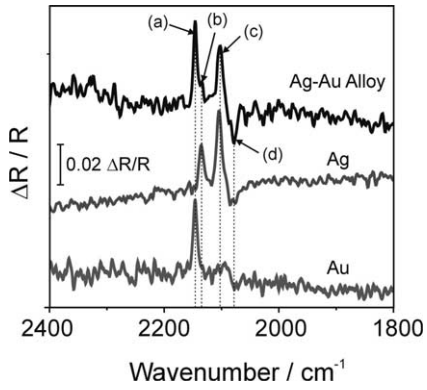

Fig. 3. Typical FTIR difference spectra obtained at $E_s = -1.00$ V during deposition of Au, Ag and Ag–Au alloy in the systems: GC/$[Au(CN)_2]^-$ (pH 14, $c_{AuCN} = 50$ mM); GC/$[Ag(CN)_2]^-$ (pH 14, $c_{AgCN} = 50$ mM) and GC/$[Ag(CN)_2]^- + [Au(CN)_2]^-$ (pH 14, $c_{AgCN} = c_{AuCN} = 50$ mM). The reference spectrum was taken at $E_r = 0$ V. Bands (a), (b), (c) and (d) are described in Table 1. Features pointing up (to $+\Delta R/R$) are due to species lost at E_s relative to E_r and features pointing down (to $-\Delta R/R$) are due to species gained at E_s relative to E_r (incidence angle: 60°).

species involved during the Ag–Au alloy deposition process in cyanide. As it can be seen in Fig. 3 and Table 1, in the case of Ag, two different complexes were observed under the experimental conditions: the complexes $[Ag(CN)_2]^-$ and $[Ag(CN)_3]^{2-}$. In the case of Au, however, only one complex was present, namely the di-cyano complex. This fact can be easily understood if the formation constants for the di-cyano complexes of both metals are considered (Table 1). Au is more electronegative than Ag, and for this reason the band corresponding to $[Au(CN)_2]^-$ appears at a higher frequency compared to that corresponding to $[Ag(CN)_2]^-$. In the spectrum obtained during the alloy deposition, all three peaks can be distinguished. Additionally, a band due to free cyanide can be observed in all cases at about 2080 cm^{-1}. All bands shown in Fig. 3 are described in Table 1.

Fig. 4 shows a series of spectra taken respectively during Ag, Au and Ag–Au alloy deposition on GC at different potentials. In the case of Ag (Fig. 4a), deposition begins at about −600 mV. Both complex species are consumed in an almost constant ratio due to the chemical equilibrium between them. However, studies performed by several Authors [18–20] suggest that the $[Ag(CN)_2]^-$ complex is the species mainly

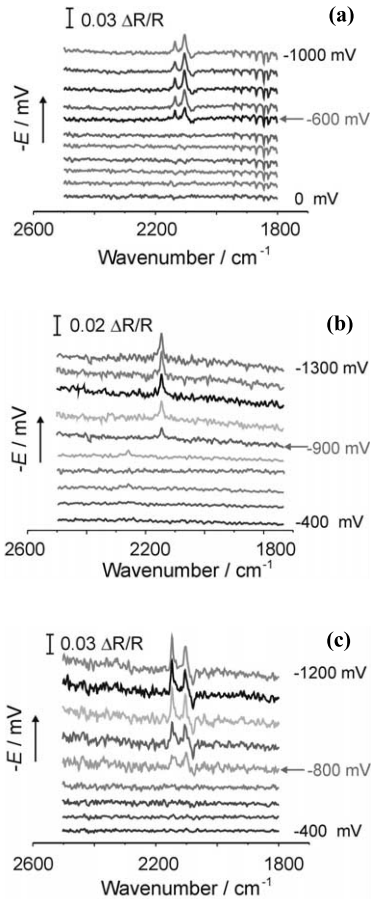

Fig. 4. FTIR difference spectra taken during: (a) Ag deposition in the system GC/$[Ag(CN)_2]^-$ (pH 14, $c_{AgCN} = 50$ mM). The potential was varied from 0 to −1.00 V in steps of −100 mV (Reference Potential: $E_r = 0$ V). (b) Au deposition in the system GC/$[Au(CN)_2]^-$ (pH 14, $c_{AuCN} = 50$ mM). The potential was varied from −0.40 to −1.30 V in steps of −100 mV ($E_r = -0.40$ V). (c) Ag–Au alloy deposition in the system GC/$[Ag(CN)_2]^- + [Au(CN)_2]^-$ (pH 14, $c_{AgCN} = c_{AuCN} = 50$ mM). The potential was varied from −0.40 to −1.20 V in steps of −100 mV ($E_r = -0.40$ V) (incidence angle: 60°).

involved in the electron transfer reaction, according to:

$$[Ag(CN)_3]^{2-} \Leftrightarrow [Ag(CN)_2]^- + CN^- \quad (2a)$$

$$[Ag(CN)_2]^- + e^- \Leftrightarrow Ag\text{–}CN^-_{(ads)} + CN^- \quad (2b)$$

$$Ag\text{–}CN^-_{(ads)} \Leftrightarrow Ag + CN^- \quad (2c)$$

Spectral studies performed during the anodic sweep indicate that Ag dissolution starts at about −400 mV. In the case of Au (Fig. 4b), changes in FTIR spectra due to deposition can be observed at those potentials more

Table 1
Spectroscopic [17] and stability [6] data of the Ag and Au cyano complexes yielding the C–N vibration bands (a), (b), (c) and (d) shown in Fig. 3

Band	Species	Wavenumber (cm^{-1})	Extinction coefficient (L/mol cm)	Cumulative formation constant
(a)	$[Au(CN)_2]^-$	2146	–	Log $K = 38.3$
(b)	$[Au(CN)_2]^-$	2132	264 ± 12	Log $K = 21.1$
(c)	$[Ag(CN)_3]^{2-}$	2103	379 ± 23	Log $K = 21.7$
(d)	CN^-	2079	29 ± 1	–

negative than −900 mV. Results obtained in the mixed solution (Fig. 4c) indicate that both metals co-deposit at $E < -800$ mV during the Ag–Au alloy formation.

Fig. 5 presents spectra taken at different times during Ag, Au and Ag–Au alloy deposition on GC at a constant potential of $E = -1.00$ V. In the case of the alloy (Fig. 5c), it can be observed that Ag and Au deposit simultaneously at all times. An additional band appears at 2138 cm^{-1}, exactly between the peaks corresponding to $[Au(CN)_2]^-$ and $[Ag(CN)_2]^-$. This band is not observed during Ag and Au deposition from the individual solutions (Fig. 5a and b) and it could be due to a shift in the C–N vibration frequency produced as a result of an interaction of the cyanide ions with both Ag and Au. This is likely to occur, given the many chemical and physical similarities between these two metals. However, a more exhaustive study is being carried out in order to be able to assign this band to a specific species. Other features can be observed at 2159, 2118 and 2092 cm^{-1}. These bands, which are just as well being currently investigated, are not characteristic for the alloy deposition, since they are also present in those spectra taken during Ag and Au deposition from the single metal solutions. As it can be seen in Fig. 5a and c, the amount of Ag complex that is consumed after 100 s for the alloy formation is lower than that consumed after the same time for pure Ag deposition; on the other hand, an opposite behaviour was observed for Au (Fig. 5b and c). Actually, in the case of Ag, these observations could be predicted from the cyclic voltammograms in Fig. 2a and b, considering that Ag deposition is diffusion controlled at $E = -1.00$ V. In the case of Au, however, FTIR spectroscopy provides important information that complements the electrochemical experiments. Apparently, Au deposition is enhanced, while Ag deposition is inhibited in the mixed electrolyte. These results, which, as mentioned before, agree very well with previous electrochemical observations, are better resumed in Fig. 6. It must be noted that the normalised reflectance change is proportional to the absorbance only at small values.

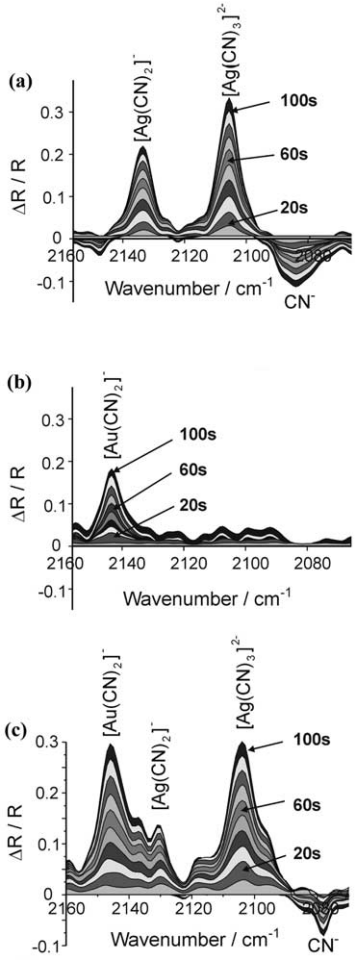

Fig. 5. FTIR difference spectra obtained at $E_s = \text{const} = -1.00$ V during: (a) Ag deposition in the system GC/$[Ag(CN)_2]^-$ (pH 14, $c_{AgCN} = 50$ mM); (b) Au deposition in the system GC/$[Au(CN)_2]^-$ (pH 14, $c_{AuCN} = 50$ mM); (c) Ag–Au alloy deposition in the system GC/$[Ag(CN)_2]^- + [Au(CN)_2]^-$ (pH 14, $c_{AgCN} = c_{AuCN} = 50$ mM). Each spectrum was obtained after 10 s acquisition time; where $t = 0$ is taken when the potential was stepped from $E_r = 0$ V to $E_s = -1.00$ V (incidence angle: 60°).

Most FTIR techniques are often applied to highly reflective and relatively smooth electrodes such as noble metals or pyrolitic graphite. In general, GC is a very convenient substrate for in situ spectroscopic experiments. Measurements on Si, however, are not so easy to perform, since this semiconductor reflects IR radiation very poorly. Nevertheless, by adequately adjusting the incident angle and/or the number of averaged interferograms, it was possible to obtain a very good signal/noise response also on this substrate, as it can be seen in Fig. 7a and b for Ag and Au deposition on n-Si(111). An important advance in recent years has been the application of FTIR to many other 'practical' electrodes, such as Pt/Ru on carbon or sol–gel TiO_2 electrodes [9].

Fig. 7a shows (as can be also seen by comparison of the cyclic voltammograms in Fig. 1a and Fig. 2a) that Ag deposition on Si begins at a higher negative potential than on GC; namely at −800 mV. This is due to the location of the flat band potential of the semiconductor in the cyanide electrolyte at pH 14, which was determined to be $E_{fb} \approx -730$ mV (Fig. 8). The flat band potential of n-Si was estimated from capacitance measurements under deep depletion conditions ($f =$ 1013 Hz) [16]. A slope of about −45 mV/pH, which deviates from the Nernstian slope of −60 mV/pH observed in many other systems, was obtained. Experimental results indicate that metal deposition on n-Si(111) only takes place after reaching the flat band potential of the semiconductor (at $E < E_{fb}$). In general, the results obtained from spectroscopic measurements during Ag, Au and Ag–Au alloy deposition on Si were quite similar to those obtained on GC. However, studies

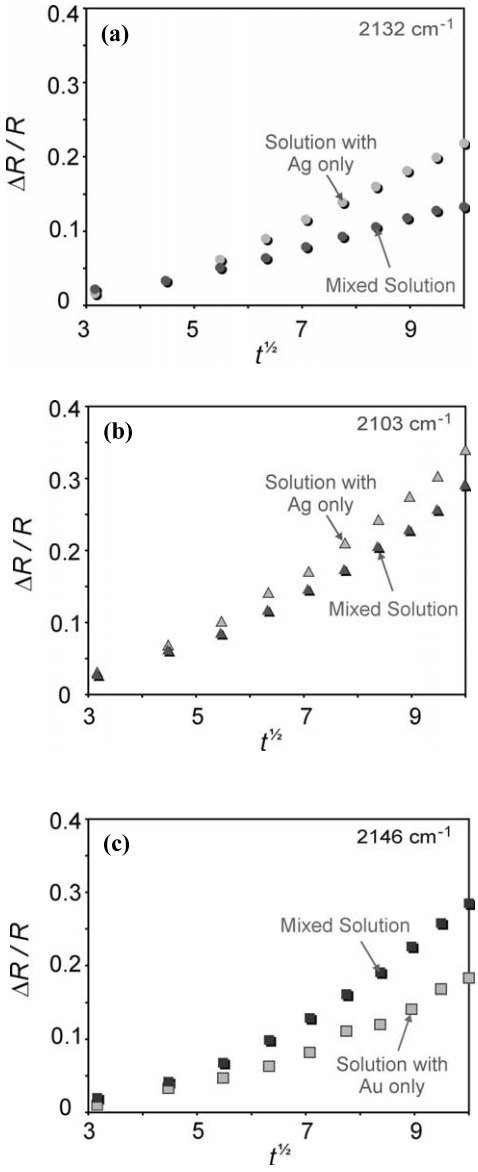

Fig. 6. Variation of the intensities of the ν(CN) bands for: (a) $[Ag(CN)_2]^-$; (b) $[Ag(CN)_3]^{2-}$; and (c) $[Au(CN)_2]^-$ during alloy and metal deposition at $E = \text{const} = -1.00$ V from the mixed and individual solutions on GC. As can be seen, Ag deposition is in somewhat inhibited (while Au deposition is enhanced) in the mixed electrolyte.

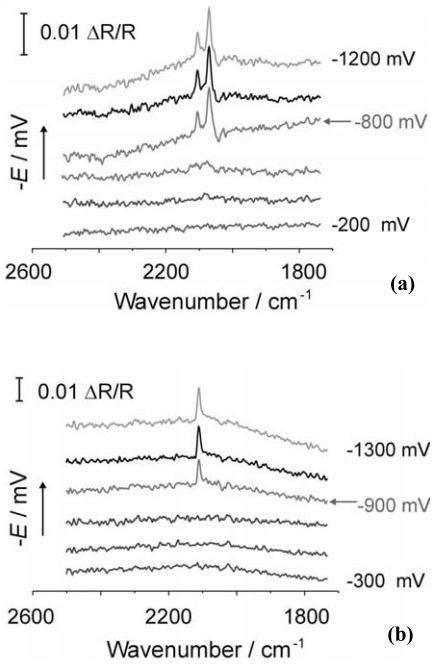

Fig. 7. FTIR difference spectra taken during: (a) Ag deposition in the system n-Si(111)/$[Ag(CN)_2]^-$ (pH 14, $c_{AgCN} = 50$ mM). The potential was varied from -0.20 to -1.20 V in steps of -200 mV (Reference Potential: $E_r = -0.20$ V); (b) Au deposition in the system n-Si(111)/$[Au(CN)_2]^-$ (pH 14, $c_{AuCN} = 50$ mM). The potential was varied from -0.30 to -1.30 V in steps of -200 mV ($E_r = -0.30$ V) (incidence angle: 40°).

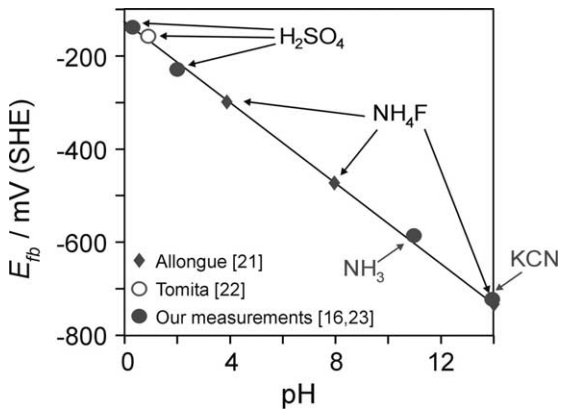

Fig. 8. Flat band potentials E_{fb} of n-Si in several electrolytes at different pH values [16,21–23]

performed on Si had one clear disadvantage: the deposits could not be dissolved electrochemically and thus, the electrode had to be dismounted and replaced after each measurement, making experiments on Si quite time-consuming and more vulnerable to experimental errors.

Due to the relatively small interaction energy between the metal adatoms and the substrate, the Ag–Au alloy deposition on n-Si(111) and GC electrodes follows a 3D island growth mechanism (Volmer-Weber mechanism) [24], as can be seen in Fig. 9a, where an AFM image of Ag–Au alloy islands deposited on n-Si(111) by applying a 20 s long pulse to $E = -1.00$ V is shown. The width/height ratios of the Ag–Au alloy clusters determined from the AFM measurements show that the growing nuclei can be considered hemispherical as assumed in most theoretical models. The observed size distribution of the clusters is characteristic for a progressive nucleation mechanism. This was also confirmed by chronoamperometric measurements. A typical current transient for Ag–Au alloy deposition in the system n-Si(111)/$[Ag(CN)_2]^-$, $[Au(CN)_2]^-$ at $E = -1.10$ V is

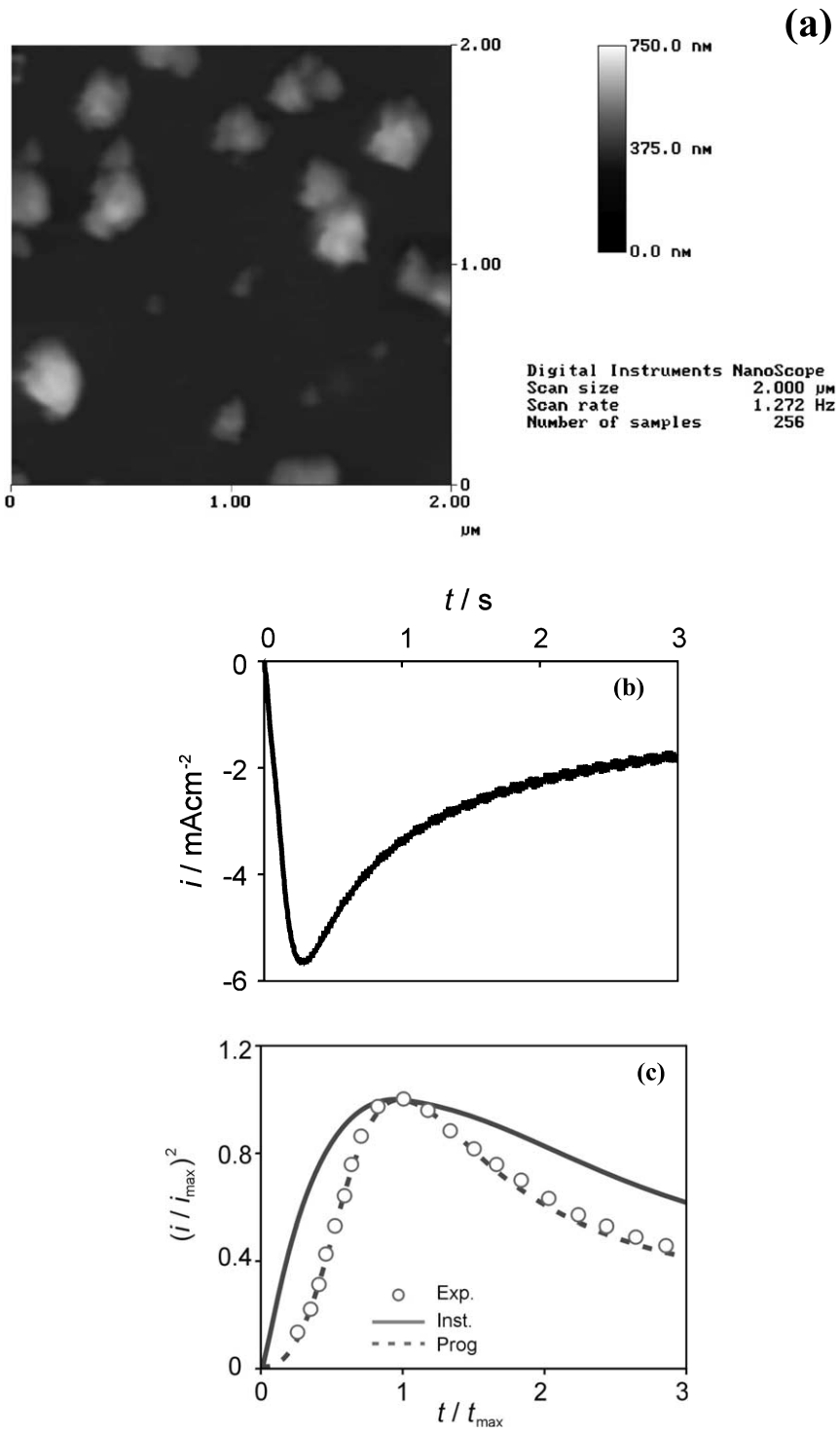

Fig. 9. (a) AFM of Ag–Au alloy clusters deposited on n-Si(111) in the system: n-Si(111)/$[Ag(CN)_2]^-$, $[Au(CN)_2]^-$ at $E = -1.00$ V and $t = 20$ s; (b) current transient for Ag–Au alloy deposition in the system n-Si(111)/$[Ag(CN)_2]^-$, $[Au(CN)_2]^-$ at $E = -1.10$ V; (c) reduced variable $(i/i_{max})^2$ vs. t/t_{max} plot of the transient in (b) compared with theoretical curves for progressive and instantaneous nucleation.

shown in Fig. 9b. This transient is plotted in Fig. 9c in reduced coordinates $(i/i_{max})^2$ versus t/t_{max} and compared with the equations for progressive and instantaneous nucleation proposed by Scharifker and Hills [25]. As it can be seen, the alloy follows a progressive nucleation mechanism, even at relatively high negative potentials. A similar behaviour was also observed for Au deposition on n-Si(111) and on n-Si(100), whilst in the case of Ag, instantaneous nucleation takes place already at −0.90 V [13,26,27]. SEM and AFM studies of Ag–Au clusters deposited at potentials more negative than −1.60 V indicate that, under these conditions, the initial

deposition in this system occurs by instantaneous nucleation. However, a quantitative analysis of current transients measured at such high negative potentials was not possible due to the overlapping hydrogen evolution current.

As mentioned before, the alloy deposition follows a 3D island growth mechanism. Thus, in order to obtain a continuous metal film, the density of nuclei must be sufficiently high for the islands to coalesce during further growth. This is particularly important for metallisation of microstructures. For depositing continuous and adherent metal films, a double pulse polarisation routine was used [13]. Initially, a density of clusters higher than 10^{10} cm^{-1} is produced under conditions of instantaneous nucleation. In a further step, the clusters grow under mixed or charge-transfer control. An example of the metallisation of a recessed n-Si/SiO_2 microstructure (prepared on the basis of Si planar technology [28]) using a double pulse polarisation routine is shown in Fig. 10.

The electronic properties of the solid state n-Si/metal and n-Si/alloy junctions were investigated in the dark by current–voltage and capacity–voltage measurements [13]. All n-Si/alloy and n-Si/metal junctions showed an ideal Schottky-diode behaviour. No significant influence of the Ag–Au alloy composition on the characteristics of deposited n-Si(111)/Ag–Au contacts was observed. A barrier height of about (0.75 ± 0.05) eV was estimated for the n-Si(111)/Ag–Au contact in all cases. The morphology and adhesion of all deposits, as well as the alloy composition, were found to be strongly dependent on the deposition potential (Fig. 11). A better adhesion of the films with a higher Au content was observed, due to the formation of a more stable Au–Si bond with a binding enthalpy of about 305 kJ/mol (binding enthalpy for Ag–Si = 178 kJ/mol) [3]. XPS surface analytical studies of deposited alloy films with a thickness between 80 and 300 nm showed that, for given deposition conditions, the alloy composition is homogeneous throughout the film and remains the same at all sputtering depths (Fig. 12).

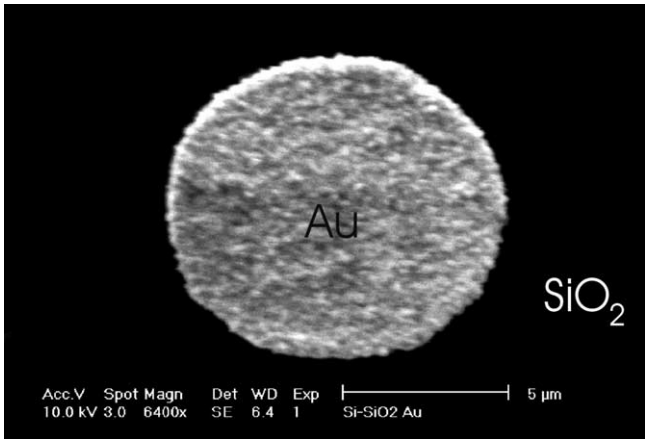

Fig. 10. Metallisation of a recessed n-Si/SiO_2 microstructure using the so-called 'capillary based electrochemical microcell' [29] and a double pulse polarisation routine. A continuous, adherent film was obtained.

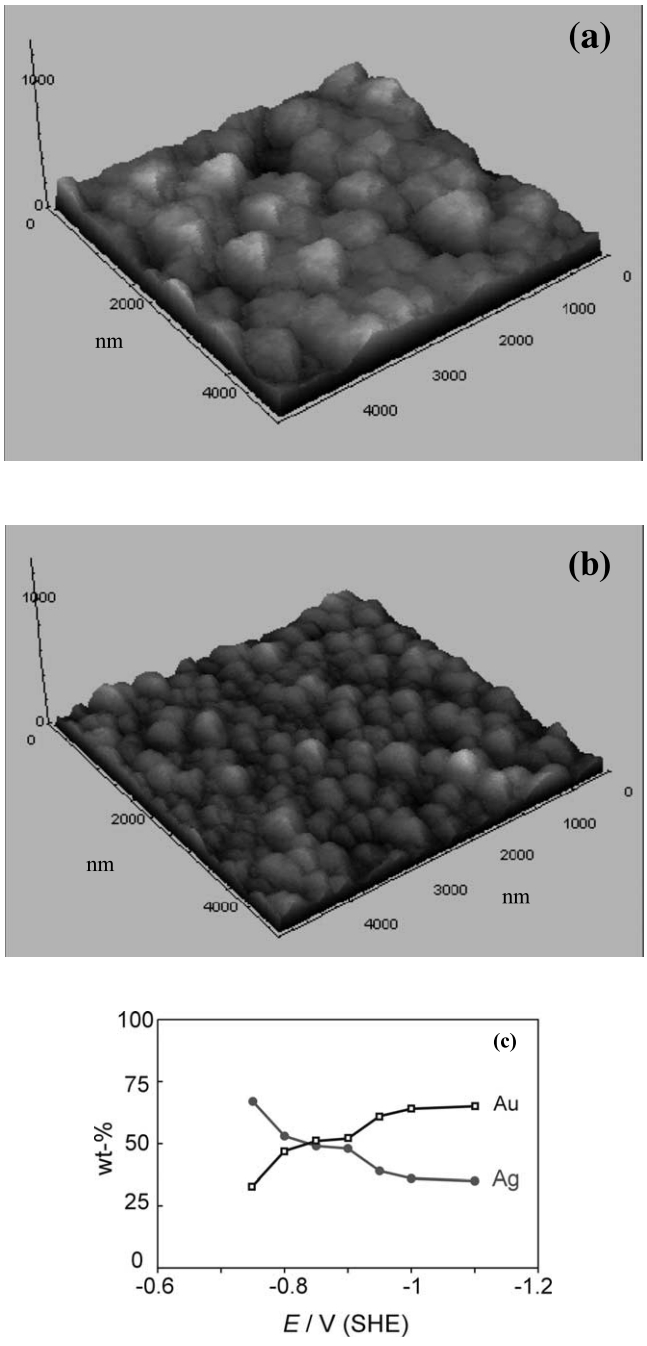

Fig. 11. (a) AFM of a Ag–Au alloy film deposited on n-Si(111) at $E = -0.80$ V. Scan size: 5 µm. (b) AFM of a Ag–Au alloy film deposited on n-Si(111) at $E = -1.10$ V. This deposit, which contains about 1.5 times more Au than the deposit shown in (a), exhibited a very good adhesion to the Si surface. Scan size: 5 µm. (c) Dependence of the composition of Ag–Au alloy clusters on the deposition potential E (obtained from EDX measurements). System: n-Si(111)/$[Ag(CN)_2]^-$, $[Au(CN)_2]^-$. Deposition time: $t = 20$ s. As can be seen, the composition, adhesion and morphology of the Ag–Au alloy deposits depend strongly on the deposition potential.

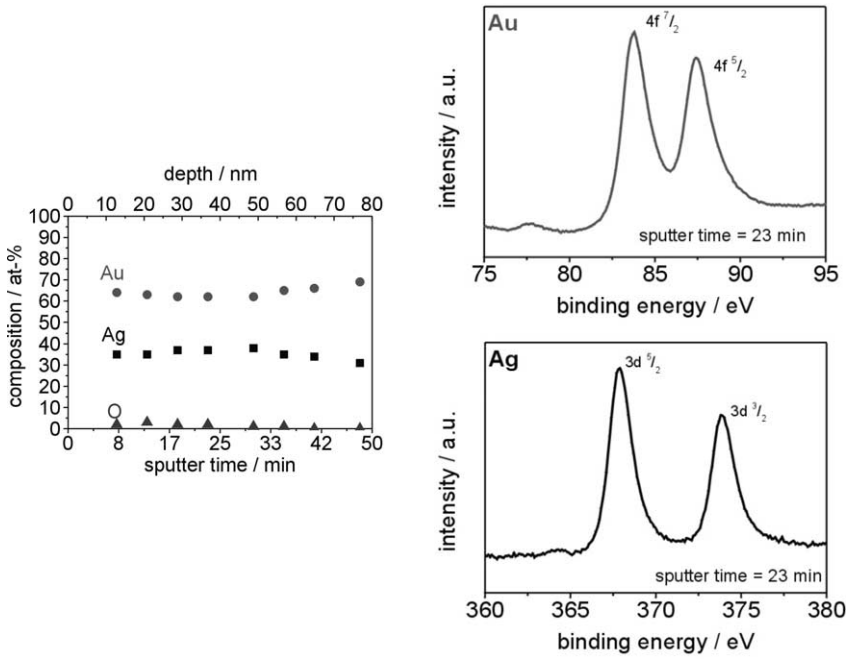

Fig. 12. XPS of a Ag–Au alloy film deposited on n-Si(111) using a double pulse polarisation routine ($E_1 = -1.60$ V, $t_1 = 50$ ms; $E_2 = -0.80$ V, $t_2 = 180$ s) in the system: n-Si(111)/$[Ag(CN)_2]^-$, $[Au(CN)_2]^-$. A homogeneous composition is observed throughout the film.

4. Conclusions

By combining electrochemical and spectroscopic techniques, the deposition of Ag, Au and Ag–Au alloys on n-Si(111) and GC electrodes, from alkaline cyanide electrolytes, was studied. Experimental results performed in one-component and mixed electrolytes containing equal amounts of AgCN and AuCN indicate that Ag deposition is thermodynamically favoured, while Au deposition is kinetically favoured. In the mixed electrolyte, Ag and Au co-deposit even in the activation region, where Ag reduction is expected to be the main reaction. The Ag–Au alloy deposition follows a progressive nucleation mechanism, even at relatively high negative potentials. In spite of the complexity of the reduction mechanism and the high tendency of the species to be adsorbed on the electrode, it is possible to control the properties of Ag–Au alloys by using appropriate deposition conditions. The morphology and adhesion of all deposits, as well as the composition of the Ag–Au alloys, were found to be strongly dependent on the deposition potential.

Acknowledgements

The Authors express their gratitude to the Ministerium für Schule und Weiterbildung, Wissenschaft und Forschung des Landes Nordrhein-Westfalen (MSWWF NRW), the Fundación Gran Mariscal de Ayacucho (FUNDAYACUCHO), the Deutscher Akademischer Austauschdienst (DAAD), and the Bundesministerium für Wirtschaft (BMWi) through the Arbeitsgemeinschaft industrieller Forschungsvereinigungen (AiF-FV-Nr.11955 N) for their financial support.

References

[1] M.V. ten Kortenaar, J.J.M. de Goeij, Z.I. Kolar, G. Frens, P.J. Lusse, M.R. Zuiddam, E. van der Drift, J. Electrochem. Soc. 148 (2001) C28.
[2] S.H. Cho, H. Kang, S.S. Wong, Y. Shacham-Diamand, MRS Bull. (1993) 31 (June).
[3] D.R. Lide (Ed.), Handbook of Chemistry and Physics, 79th ed., CRC Press, Boca Raton, FL, 2000.
[4] Y. Borensztein, R. Alameh, Surf. Sci. Lett. 274 (1992) 509.
[5] A. Samsavar, E.S. Hirschhorn, F.M. Leibsle, T.C. Chiang, Phys. Rev. Lett. 63 (1989) 2830.
[6] Managing Cyanide in Metal Finishing, EPA 625/R-99/009, U.S. Environmental Protection Agency (Dec 2000).
[7] G. Oskam, J.G. Long, A. Natarajan, P.C. Searson, J. Phys. D: Appl. Phys. 31 (1998) 1927.
[8] A. Bewick, K. Kunimatsu, B.S. Pons, Electrochim. Acta 25 (1980) 465.
[9] P. Christensen, A. Hamnett, Electrochim. Acta 45 (2000) 2443.
[10] R. Ortiz, O.P. Márquez, J. Márquez, C. Gutiérrez, J. Phys. Chem. 100 (1996) 8389.
[11] R. Ortiz, A. Cuesta, O.P. Márquez, J. Márquez, J.A. Mendez, C. Gutiérrez, J. Electroanal. Chem. 465 (1999) 234.
[12] T. Davidson, B.S. Pons, A. Bewick, P.P. Schmidt, J. Electroanal. Chem. 125 (1981) 237.
[13] K. Márquez, G. Staikov, J.W. Schultze, Trans. Inst. Met. Finish. 80 (3) (2002) 73.
[14] L.F. D'Elia, R. Ortíz, O.P. Márquez, J. Márquez, J. Electrochem. Soc. 148 (2001) 297.
[15] D.M. MacArthur, J. Electrochem. Soc. 119 (1972) 672.
[16] K. Márquez, G. Staikov, J.W. Schultze, unpublished results.
[17] L.H. Jones, R.A. Penneman, J. Chem. Phys. 22 (1954) 965.

[18] W. Vielstich, H. Gerischer, Z. Phys. Chem. NF4 (1955) 10.
[19] H. Gerischer, Chem. Ing. Tech. 36 (1964) 666.
[20] H. Baltruschat, W. Vielstich, J. Electroanal. Chem. 154 (1983) 141.
[21] P. Allongue, V. Kieling, H. Gerischer, Electrochim. Acta 40 (1995) 1353.
[22] E. Tomita, N. Matsuda, K. Itaya, J. Vac. Sci. Technol. A8 (1990) 534.
[23] R. Krumm, B. Guel, C. Schmitz, G. Staikov, Electrochim. Acta 45 (2000) 73.
[24] E. Budevski, G. Staikov, W.J. Lorenz, Electrochemical Phase Formation And Growth, VCH, Weinheim, 1996.
[25] B.R. Scharifker, G.J. Hills, Electrochim. Acta 28 (1983) 879.
[26] G. Oskam, P. Searson, Surf. Sci. 446 (2000) 103.
[27] G. Oskam, P. Searson, J. Electrochem. Soc. 147 (2000) 2199.
[28] G. Buß, M.J. Schöning, H. Lüth, J.W. Schultze, Electrochim. Acta 44 (1999) 3899.
[29] M.M. Lohrengel, A. Moehring, M. Pilaski, Electrochim. Acta 47 (2001) 137.